Preprints of the 21st IFAC World Congress (Virtual)
Berlin, Germany, July 12-17, 2020

Modified preactuation tracking control for LPV systems with application to boost converters

Shota Miyoshi * **Wataru Ohnishi** * **Takafumi Koseki** *
Motoki Sato **

* *The University of Tokyo, Tokyo, Japan, (e-mail: miyoshi@koseki.t.u-tokyo.ac.jp, ohnishi@ieee.org, takafumikoseki@ieee.org)*
** *Toyo Denki Seizo K.K, Tokyo, Japan(e-mail: satoum@toyodenki.co.jp)*

Abstract: Boost converters are usually employed as constant or discrete variable voltage sources. They are expected as a continuously variable voltage source for electric drives (based on pulse-amplitude modulation control), or for reduction of the size of energy buffer components for mass motor drives. When changing the output voltage of boost converters according to the duty ratio, the nonlinear and nonminimum phase characteristics of boost converters cause undershoots. This study was devoted to extending the technique known as preactuated multirate feedforward (PMF), which can effectively compensate for the effects caused by nonminimum phase characteristics in boost converters. PMF was originally considered for linear time-invariant systems. In this study, the technique was extended to linear parameter-varying systems by the interpolation method. Simulation and experimental results verified the effectiveness of the proposed approach.

Keywords: Boost converter, Variable voltage, Feedforward Control, Trajectory tracking, Precise control, Preactuation

1. INTRODUCTION

Boost converters are widely applied in industrial and commercial environments. In this study, we focused on two critical points of boost converters: downsizing their components and achieving a higher tracking performance. Boost converters include expensive components such as a capacitor and an inductor. Thus, boost converters will greatly benefit from smaller sizes of these components. Previous studies (Takei et al. (2014)) showed that volume reduction of components in boost converters can be achieved by feedforward control of the output voltage.

Moreover, a higher voltage tracking performance of boost converters enables the realization of high-performance pulse amplitude modulation (PAM) converters. PAM converters can achieve optimal usage of the DC link voltage of converters and inverters and save energy in power converters (Schwager et al. (2014)). Concerning boost converters, previous studies aimed to improve the voltage-reference tracking performance. In this field, techniques based on sliding mode control (Wai and Shih (2011)), model predictive control (Karamanakos et al. (2014)), and deadbeat control (Mushi et al. (2017)) were developed to solve the aforementioned critical points. Another approach based on continuous-time models was reported. By applying state-space averaging (Wester and Middlebrook (1972)), the boost converters were treated as continuous systems. Then, two-degree-of-freedom (2-DOF) control can be applied to improve the tracking performance by feedforward control.

For the reasons mentioned above, we focused on the feedforward control of boost converters and developed an extension of preactuated multirate feedforward (PMF) control (Ohnishi et al. (2019)) for them. The transfer function of a boost converter was necessary for designing the feedforward controller. The linearized plant model of a boost converter was described through a linear parameter-varying (LPV) model (Olalla et al. (2011)) calculated by the state-space averaging method. This model has nonminimum phase zeros that have a positive real part in the averaged plant model. Owing to the points mentioned above, it is difficult to achieve a faster response from boost converters. Previous studies (Takei et al. (2014)) proposed a multirate feedforward control method that ignored unstable zeros to reduce the dimensions of the boost converters. PMF is a powerful technique for linear time-invariant (LTI) nonminimum phase systems to suppress undershoots caused by nonminimum phase zeros. We propose a method based on an internal division of two control inputs that are created by the approximation of LPV systems at the starting and end points of voltage tracking. Through this method, PMF can be effectively applied to LPV systems, especially to boost converters.

The present manuscript comprises six sections. In Section 2, a continuous model of transient characteristics for boost converters derived by applying state-space averaging is de-

Copyright lies with the authors

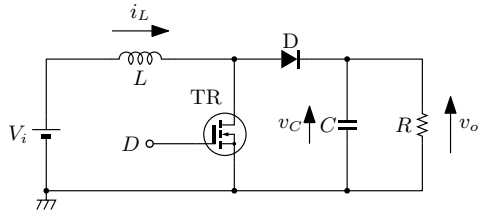

(a) Circuit schematic.

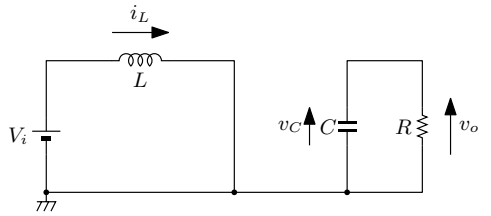

(b) State 1: TR is on.

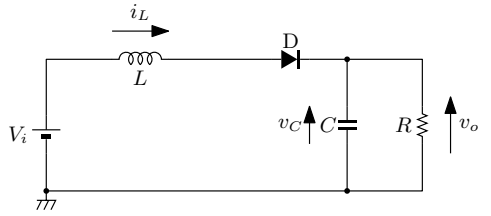

(c) State 2: TR is off.

Fig. 1. A circuit schematic of a boost converter and its switching states.

scribed. In Section 3, we extend PMF. Section 4 describes the proposed method by applying the preactuated feedforward to averaged continuous-time models. In Section 5, numerical simulation results of the proposed control law are reported and discussed. Finally, Section 6 concludes this paper.

2. TRANSIENT CHARACTERISTICS OF BOOST CONVERTERS

A circuit schematic of a boost converter is shown in Fig. 1 (a). This boost converter has two operation states shown in Fig. 1 (b) and (c) when the transistor is on and off respectively. To analyze the dynamic characteristics of the boost converter, state-space averaging (Wester and Middlebrook (1972)) is applied.

2.1 State-space averaging

State-space averaging (Wester and Middlebrook (1972), Erickson and Maksimovic (2001)) is an approximation method to address a periodic discrete system that has switches as a continuous system. This method is effective for describing the performance of the system for a longer enough time interval than the switching period. The averaged state of the system is obtained by the average of each state-space weighted by the time interval that each state has in one period.

2.2 Application of state-space averaging to boost converters

Fig. 1 (a) shows that the circuit in a boost converter has two closed loops. Two state variables can be taken from each closed loop. In this paper, the current of the inductor i_L and the voltage of the capacitor v_C are taken as state variables. Let the state variable be $\boldsymbol{x} = (i_L \quad v_C)^T$, the input variable be $u = V_i$, and the output variable be $\boldsymbol{y} = (i_L \quad v_o)^T$.

When the transistor (TR) is on, as shown in Fig. 1 (b), the state-space can be expressed as

$$\dot{\boldsymbol{x}} = \begin{pmatrix} 0 & 0 \\ 0 & -\dfrac{1}{CR} \end{pmatrix} \boldsymbol{x} + \begin{pmatrix} \dfrac{1}{L} \\ 0 \end{pmatrix} u =: \boldsymbol{A}_1 \boldsymbol{x} + \boldsymbol{b}_1 u, \tag{1}$$

$$\boldsymbol{y} = \begin{pmatrix} 1 & 0 \\ 0 & 1 \end{pmatrix} \boldsymbol{x} =: \boldsymbol{C}_1 \boldsymbol{x}. \tag{2}$$

Correspondingly, when TR is off, as shown in, Fig. 1 (c), the state-space can be expressed as

$$\dot{\boldsymbol{x}} = \begin{pmatrix} 0 & -\dfrac{1}{L} \\ \dfrac{1}{C} & -\dfrac{1}{CR} \end{pmatrix} \boldsymbol{x} + \begin{pmatrix} \dfrac{1}{L} \\ 0 \end{pmatrix} u =: \boldsymbol{A}_2 \boldsymbol{x} + \boldsymbol{b}_2 u, \tag{3}$$

$$\boldsymbol{y} = \begin{pmatrix} 1 & 0 \\ 0 & 1 \end{pmatrix} \boldsymbol{x} =: \boldsymbol{C}_2 \boldsymbol{x}. \tag{4}$$

Let $D = T_{on}/T$ be the duty ratio, where T denotes the switching period of TR and T_{on} denotes the time interval in which TR is on in one switching period. Let also $D' = 1 - D$ be the complementary duty ratio. The averaged state-space of the boost converter is obtained as follows:

$$\boldsymbol{A} = D\boldsymbol{A}_1 + D'\boldsymbol{A}_2,\ \boldsymbol{b} = D\boldsymbol{b}_1 + D'\boldsymbol{b}_2,$$
$$\boldsymbol{C} = D\boldsymbol{C}_1 + D'\boldsymbol{C}_2$$

and

$$\dot{\boldsymbol{x}} = \boldsymbol{A}(D)\boldsymbol{x} + \boldsymbol{b}(D)u \tag{5}$$

$$\boldsymbol{y} = \boldsymbol{C}(D)\boldsymbol{x} \tag{6}$$

(5), (6) shows that the state-space of the boost converter varies drastically by changing the duty ratio D.

2.3 Steady-state and small-signal transfer functions of the boost converter

State-space averaging provides the averaged values of a system when the changing speed of the system is sufficiently slower than the switching period of the states of the system.

The steady state of the system can be obtained by setting $\dot{\boldsymbol{x}} = \boldsymbol{0}$ in (5). From (5), $\boldsymbol{x} = -\boldsymbol{A}^{-1}\boldsymbol{b}\boldsymbol{u}$ is obtained. Substituting it into (6), the steady state is obtained.

$$\boldsymbol{y}_o = -\boldsymbol{C}\boldsymbol{A}^{-1}\boldsymbol{b}u$$
$$\begin{pmatrix} I_L \\ V_o \end{pmatrix} = \frac{V_i}{D'^2 R} \begin{pmatrix} 1 \\ D'R \end{pmatrix} \tag{7}$$

Dynamics of boost converters are described by their averaged state-space (5). However, (5) includes the product of D and the state variables $\boldsymbol{x}$. Therefore, responses of state spaces against the change of duty ratio D become nonlinear.

Next, the small-signal transfer functions are obtained at an operation point. Let the operation point be $(D_0, u_0, \boldsymbol{x}_0, \boldsymbol{y}_0)$ and let the small signals be $D = D_0 + \Delta D$, $u = u_0 + \Delta u$,

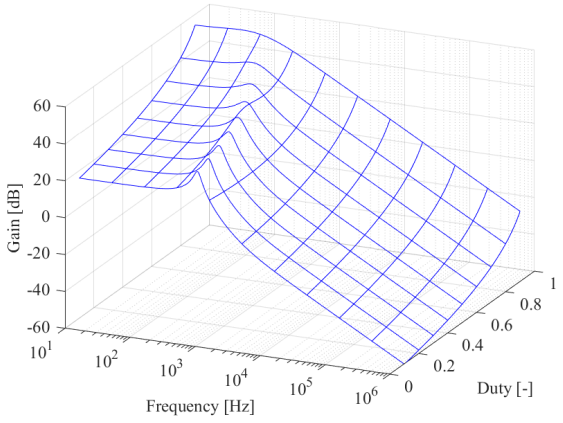

Fig. 2. Gain of the output-voltage transfer function for the averaged boost converter.

$\boldsymbol{x} = \boldsymbol{x}_0 + \Delta\boldsymbol{x}$, $\boldsymbol{y} = \boldsymbol{y}_0 + \Delta\boldsymbol{y}$. Substituting the variables in (5) and (6), we obtain

$$\frac{d}{dt}\Delta\boldsymbol{x} = \boldsymbol{A}\Delta\boldsymbol{x} + \boldsymbol{b}\Delta u + \left(\frac{\partial \boldsymbol{A}}{\partial D}\boldsymbol{x} + \frac{\partial \boldsymbol{b}}{\partial D}u\right)\Delta D, \tag{8}$$

$$\Delta\boldsymbol{y} = \boldsymbol{C}\boldsymbol{x} + \frac{\partial \boldsymbol{C}}{\partial D}\boldsymbol{x}\Delta D. \tag{9}$$

The Laplace transform of (8) and (9) generates the small-signal transfer functions with respect to ΔD

$$\frac{\Delta\boldsymbol{y}}{\Delta D} = \boldsymbol{C}(s\boldsymbol{I} - \boldsymbol{A})^{-1}\left(\frac{\partial \boldsymbol{A}}{\partial D}\boldsymbol{x} + \frac{\partial \boldsymbol{b}}{\partial D}u\right) + \frac{\partial \boldsymbol{C}}{\partial D}\boldsymbol{x}. \tag{10}$$

(10) is concretely written as

$$\frac{\Delta V_o}{\Delta D} = \frac{V_i}{D'^2}\frac{1 - \dfrac{L}{D'^2R}s}{1 + \dfrac{L}{D'^2R}s + \dfrac{LC}{D'^2}s^2}, \tag{11}$$

$$\frac{\Delta I_L}{\Delta D} = \frac{2V_i}{D'^3R}\frac{1 + \dfrac{CR}{2}s}{1 + \dfrac{L}{D'^2R}s + \dfrac{LC}{D'^2}s^2}. \tag{12}$$

The poles of (11) and (12) coincide, and their values are

$$p_\pm = -\frac{1}{2CR} \pm \sqrt{\frac{1}{(2CR)^2} - \frac{D'^2}{LC}}. \tag{13}$$

A zero of (11) is

$$z_v = \frac{D'^2R}{L} \tag{14}$$

and a zero of (12) is

$$z_i = -\frac{2}{CR}. \tag{15}$$

(11) has a positive zero according to (14) and therefore the system are nonminimum phase.

Fig.2 shows the gain of the averaged LPV transfer function of the output voltage expressed as (11). A drastic change of dynamics is observed in Fig.2 when changing the duty ratio.

In this study, the averaged state space defined by (5) and (6), and the small-signal transfer function expressed in (11) and (12) were used to design controllers and run mathematical simulations.

3. PREACTUATED MULTIRATE FEEDFORWARD CONTROL

PMF (Ohnishi et al. (2019)) is a feedforward method that carries out perfect tracking for nonminimum-phase LTI systems. It is based on two techniques: preactuation and multirate feedforward (MRFF). A block diagram of PMF is shown in Fig. 3.

3.1 Preactuation

Preactuation (Devasia et al. (1996)) is a feedforward method that uses future reference output trajectories to design control input trajectories. By actuating before the output change begins, a perfect tracking feedforward control input can be obtained in nonminimum-phase LTI systems.

Let (16) be the transfer function of a LTI plant to be applied preactuation.

$$\frac{Y(s)}{U(s)} = K_0\frac{B(s)}{A(s)} = K_0\frac{s^m + b_{m-1}s^{m-1} + \cdots + b_0}{s^n + a_{n-1}s^{n-1} + \cdots + a_0} \tag{16}$$

where $m < n$ and $B(s)$ has at least 1 nonminimum phase zero. Let $X(s)$ be the state variable to satisfy the equation (17) with respect to the output variable $Y(s)$ of the transfer function (16).

$$X(s) = \frac{1}{B(s)}Y(s). \tag{17}$$

Then, expand $F(s) = 1/B(s)$ into a partial fraction and divide the terms into two parts, namely stable part $F_{st}(s)$ and unstable parts $F_{ust}(s)$

$$F(s) = F_{st}(s) + F_{ust}(s). \tag{18}$$

One-sided inverse Laplace transform of the convolution of $F(s)$ and $X(s)$ is required to achieve perfect tracking of $r(t)$. This transform will diverge when $t \to \infty$ owing to the instability of $F_{ust}(s)$.

To accomplish stable inversion, the following double-sided Laplace transform is applied (Sogo (2010)).

$$G(s) = \bar{\mathcal{L}}[g(t)] := \int_{-\infty}^{+\infty} e^{-st}g(t)dt. \tag{19}$$

If we assume $f_{st}(t)$ and $\bar{f}_{ust}(t)$ and the one-sided inverse Laplace transform of $F_{st}(s)$ and $F_{ust}(-s)$, $x_d(t)$, which is the stable inversion of $r(t)$, is given by

$$x_d(t) = \int_{-\infty}^{t} f_{st}(t-\tau)r(\tau)d\tau + \int_{-\infty}^{\bar{t}} \bar{f}_{ust}(\bar{t}-\tau)r(-\tau)d\tau\Big|_{\bar{t}=-t}. \tag{20}$$

The second term of (20) is the part that calculates the convolution for the unstable part of the transfer function by time axis inversion. The reference trajectory $r(t)$ is inverted into $r(-t)$ and convoluted with the s-domain inverted transfer function $\bar{f}_{ust}(\bar{t}) = \mathcal{L}^{-1}[F_{ust}(-s)]$. Then, the time axis of the result is inverted $\bar{t} = -t$ again. Note that $x(t) \neq 0$ even though $t < 0$ because the lower end of integration is $-\infty$. Thus, the state variable $x(t)$ needs to change before the beginning of the reference trajectory $r(t)$.

3.2 Multirate feedforward

Multirate feedforward (Fujimoto et al. (2001)) is a effective feedforward method that suppresses positive zeros appear-

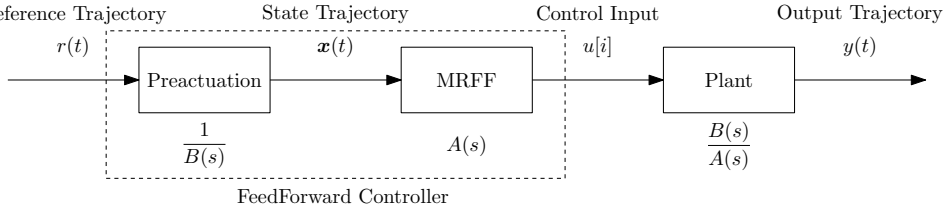

Fig. 3. Block diagram of the whole structure of a PMF control system.

ing when discretizing continuous-time transfer functions. When the order of the system is N, the inverted system can be calculated by setting the control-input sampling rate to N times the output sampling rate. Thus, perfect tracking at every output sampling point can be achieved.

Let

$$\dot{\boldsymbol{x}}(t) = \boldsymbol{A}_c\boldsymbol{x}(t) + \boldsymbol{b}_c\boldsymbol{x}(t). \tag{21}$$

be a continuous-time state space and N be the order of system. Let the sampling rate of the control input be N times the output sampling rate. Applying the zero-order-hold discretization method, we obtain

$$\boldsymbol{x}((i+1)T_r) = e^{T_r\boldsymbol{A}_c}\boldsymbol{x}(iT_r) + \sum_{k=1}^{N} u_k(iT_r)\int_{(i+\frac{k-1}{N})T_r}^{(i+\frac{k}{N}))T_r} e^{((i+1)T_r-\tau)A_c}\boldsymbol{b}_c d\tau \tag{22}$$

Assuming

$$\boldsymbol{A}_s = e^{\frac{1}{N}T_r\boldsymbol{A}_c},\ \boldsymbol{b}_s = \int_0^{\frac{1}{N}T_r} e^{\tau\boldsymbol{A}_c}\boldsymbol{b}_c d\tau \tag{23}$$

then

$$\boldsymbol{A} = \boldsymbol{A}_s^N,\ \boldsymbol{B} = \begin{pmatrix}\boldsymbol{A}_s^{N-1}\boldsymbol{b}_s & \boldsymbol{A}_s^{N-2}\boldsymbol{b}_s & \cdots & \boldsymbol{b}_s\end{pmatrix}$$

is obtained. Note that $\boldsymbol{B}$ is nonsingular when the state, described by $\boldsymbol{A}_s$, $\boldsymbol{b}_s$, becomes controllable. From (22), the multirate control input is obtained.

$$\begin{aligned}\boldsymbol{x}[i+1] &= \boldsymbol{A}\boldsymbol{x}[i] + \boldsymbol{B}\boldsymbol{u}[i]\\ \boldsymbol{u}[i] &= \boldsymbol{B}^{-1}(\boldsymbol{x}[i+1] - \boldsymbol{A}\boldsymbol{x}[i])\\ \Leftrightarrow \boldsymbol{u}[i] &= \boldsymbol{B}^{-1}(I - z^{-1}\boldsymbol{A})\boldsymbol{x}[i+1].\end{aligned} \tag{24}$$

4. MODIFICATION OF PREACTUATION IN BOOST CONVERTERS

In this section, we describe how PMF was applied in boost converters.

4.1 Conventional method

We applied two conventional methods to design a varying voltage trajectory. The first method was a step-shaped trajectory, whereas the second was a polynomial trajectory. A polynomial trajectory $v_r(t) = a_n t^n + \cdots + a_0$ was designed by solving the following equation (25) of boundary conditions:

$$\begin{cases} V_r(0) = V_{start}, \\ V_r^{(k)}(0) = 0, & 1 \le k \le (n-1)/2, \\ V_r(T_r) = V_{end}, \\ V_r^{(k)}(T_r) = 0, & 1 \le k \le (n-1)/2 \end{cases} \tag{25}$$

In (25), T_r denotes the rise time of the trajectory and $V_r^{(k)}(t)$ denotes the k-th-order derivative of $V_r(t)$.

4.2 Proposed method

The proposed method consists of applying PMF to a polynomial output voltage trajectory for precisely controlling the output voltage of the boost converter. Because of the LPV characteristics of the boost converter, PMF cannot be applied directly; hence, nonlinearity compensation is required. The proposed compensation method is described in the next section.

(1) **Step 1: PMF at starting point** To suppress an undershoot in the starting point of the voltage change, PMF using a small-signal approximation at the starting point of voltage change $V_r = V_{start}$ is applied to the polynomial trajectory. A steady-state error of duty ratio occurs at the endpoint of voltage change that is away from the approximation center owing to the approximation of the LPV system as an LTI system. To compensate for this error, the obtained duty trajectory is multiplied by $D_{end,LPV}/D_{end,LTI}$, where $D_{end,LTI}$ denotes the duty ratio at the endpoint of the trajectory obtained by LTI approximation and $D_{end,LPV}$ denotes the duty ratio obtained by an LPV model of the boost converter.

(2) **Step 2: PMF at endpoint** To suppress an overshoot in the endpoint of the voltage change, PMF using a small-signal approximation at the endpoint of the voltage change $V_r = V_{end}$ is applied to the polynomial trajectory that is obtained by solving (25).

(3) **Step 3: PMF interpolation** The duty trajectory is created by interpolation of steps 1 and 2. The whole duty trajectory generation system is shown in Fig. 4. The interpolated duty trajectory $D(t)$ is calculated by the following expression (26) by using $D_1(t)$ and $D_2(t)$.

$$D(t) = \frac{D_1(t)(D_{end} - D_2(t)) + D_2(t)(D_1(t) - D_{start})}{(D_1(t) - D_{start}) + (D_{end} - D_2(t))} \tag{26}$$

(26) expresses the average of $D_1(t)$ and $D_2(t)$ weighted by the closeness of the starting point $D_1(t) - D_{start}$ or that of the endpoint $D_2(t) - D_{end}$ of the trajectories, as shown in Fig. 5.

5. NUMERICAL SIMULATION AND EXPERIMENTAL VERIFICATION

This study complies with the philosophy of 2-DOF control in which trajectory tracking performance must be achieved by feedforward control. Thus, numerical evaluations and experimental verifications were conducted with only feedforward control to clarify its effect.

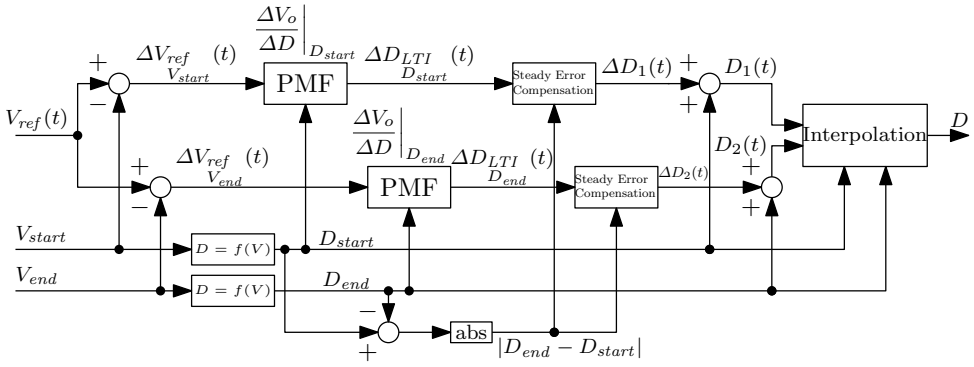

Fig. 4. Duty trajectory generation from the output voltage trajectory by PMF at the starting point or endpoint.

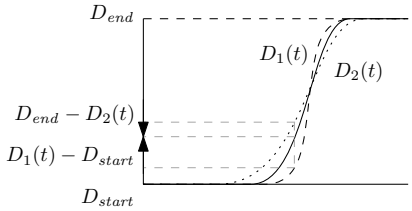

Fig. 5. Trajectory generation by interpolation of two trajectories.

Table 1. Conditions of the converter circuit.

Parameter	Value
Inductance L	400 μH
ESR of inductor r_L	0.10 Ω
Capacitance C	89 μF
Load resistance R	10 Ω
Input voltage V_i	5 V
Output voltage V_o	10 V $\rightarrow$ 15 V
Rise time T_r	2 ms
Order of polynomial trajectory	9

The whole structure of the control system used for numerical and experimental evaluations is shown in Fig.3.

5.1 Conditions of the converter circuit

Circuit parameters used for numerical simulations and experimental verifications are shown in Table 1.

5.2 Numerical simulations

The numerical simulation results are shown in Fig. 6, where "Reference" plot denotes the reference trajectory of the proposed modified PMF method.

Switching ripples in these plots were averaged every 1 period of switching cycles to evaluate the performance of trajectory tracking. Note that the 98-% settling time, as well as overshoots and undershoots of the output voltage obtained by simulation are shown in Table 2. The voltage tracking errors are shown in Table 3.

The maximum values of overshoot and voltage trajectory tracking error became smaller when applying the proposed method, thereby confirming its superiority. Especially, PMF interpolation gave rise to significantly smaller overshoot, undershoot, and tracking error.

Table 2. Summary of simulation results.

Method	undershoot [%]	overshoot [%]	settling time [ms]
Step input	10.0	27.1	5.2
Polynomial input	1.3	22.1	6.2
PMF at start	0.3	9.3	4.6
PMF at end	0.0	3.7	5.2
PMF interpolation	3.6	2.1	4.4

Table 3. Simulation results of maximum tracking error.

Method	Maximum tracking error [V]
Step input	1.36
PMF interpolation	0.33

5.3 Experimental verification

For experimental verification, the circuit shown in Fig. 1 (a) was implemented. Experimental equipment is also shown in Fig. 8.

Experimental results are shown in Fig. 7. Through PMF interpolation, overshoots in output voltage and inductor current significantly decreased. Observing the averaged value of output voltage shown in Fig. 7 (c) and (d), we can conclude that the waveform was similar to the corresponding numerical simulation. The feasibility and effectiveness of the proposed method was confirmed by this result.

6. CONCLUSION

Extension of PMF to nonlinear switching systems based on state-space averaging and linearization was developed and applied to boost converters. Numerical simulations showed that the proposed method decreases the tracking error significantly. Moreover, improved tracking performance was obtained in boost converters by applying the proposed PMF method.

Experimental verification showed similar results to numerical simulations. However, steady error appeared by parameter variation of the converter circuit because of the lack of feedback control.

The following future extensions of this study are considered. First, the development of a feedback controller is needed to suppress the steady error. To this end, a 2-DOF control must be established. Second, a preactuated

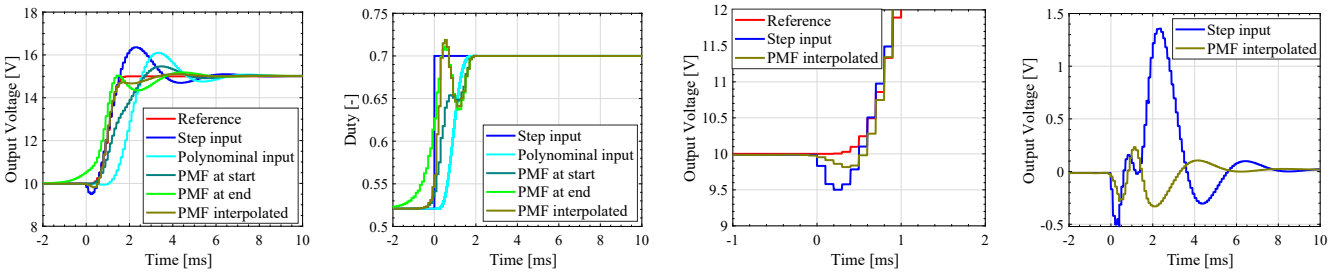

(a) Output voltage. (b) Control input duty ratio. (c) Magnified output voltage. (d) Output-voltage tracking error.

Fig. 6. Numerical simulation results of PMF applied to a boost converter.

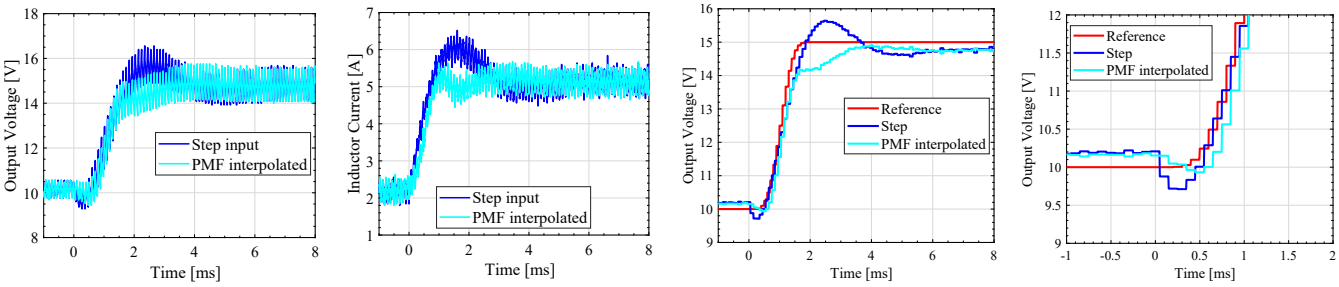

(a) Output voltage. (b) Inductor current. (c) Averaged output voltage. (d) Averaged output voltage magnified.

Fig. 7. Experimental results of PMF applied to a boost converter.

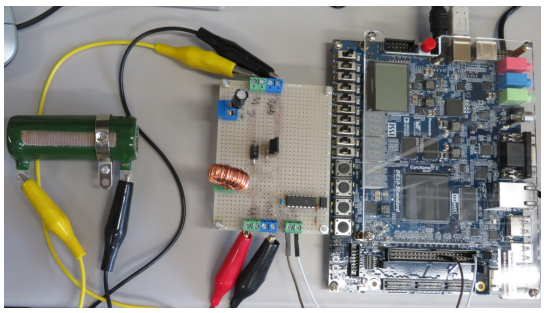

Fig. 8. Experimental bench.

controller for better tracking performance based on the direct use of the LPV system will also be developed.

REFERENCES

Devasia, S., Chen, D., and Paden, B. (1996). Nonlinear inversion-based output tracking. *IEEE Transactions on Automatic Control*, 41(7), 930–942.

Erickson, R.w. and Maksimovic, D. (2001). *Fundamentals of Power Electronics Second Edition*. Springer.

Fujimoto, H., Hori, Y., and Kawamura, A. (2001). Perfect Tracking Control Method Based on Multirate Feedforward Control. *IEEE Transactions on Industrial Electronics*, 48(3), 636–644.

Karamanakos, P., Geyer, T., and Manias, S. (2014). Direct voltage control of DC-DC boost converters using enumeration-based model predictive control. *IEEE Transactions on Power Electronics*, 29(2), 968–978.

Mushi, A., Nagai, S., Obara, H., and Kawamura, A. (2017). Fast and Robust Nonlinear Deadbeat Current Control for Boost Converter. *IEEJ Journal of Industry Applications*, 6(5), 311–319.

Ohnishi, W., Beauduin, T., and Fujimoto, H. (2019). Preactuated Multirate Feedforward Control for Independent Stable Inversion of Unstable Intrinsic and Discretization Zeros. *IEEE/ASME Transactions on Mechatronics*, 24(2), 863–871.

Olalla, C., Queinnec, I., and Leyva, R. (2011). Robust gain-scheduled control of dc-dc converters: An LMI approach. *Proceedings of the IEEE International Conference on Control Applications*, 1425–1430.

Schwager, L., Tuysuz, A., Zwyssig, C., and Kolar, J.W. (2014). Modeling and comparison of machine and converter losses for PWM and PAM in high-speed drives. *IEEE Transactions on Industry Applications*, 50(2), 995–1006.

Sogo, T. (2010). On the equivalence between stable inversion for nonminimum phase systems and reciprocal transfer functions defined by the two-sided Laplace transform. *Automatica*, 46(1), 122–126.

Takei, D., Fujimoto, H., and Hori, Y. (2014). Load current feedforward control of boost converter for downsizing output filter capacitor. *IECON Proceedings (Industrial Electronics Conference)*, 135(5), 1581–1586.

Wai, R.J. and Shih, L.C. (2011). Design of voltage tracking control for DC-DC boost converter via total sliding-mode technique. *IEEE Transactions on Industrial Electronics*, 58(6), 2502–2511.

Wester, G.W. and Middlebrook, R.D. (1972). Low-frequency characterization of switched DC-DC converters. *PESC Record - IEEE Annual Power Electronics Specialists Conference*, 1972-Janua, 9–20.